Tikrit Journal of Engineering Sciences (2025); 32(3): 1739
DOI: http://doi.org/10.25130/tjes.32.3.17

IRAQI Academic Scientific Journals

ISSN: 1813-162X (Print); 2312-7589 (Online)
Tikrit Journal of Engineering Sciences
available online at: http://www.tj-es.com

TJES Tikrit Journal of Engineering Sciences

# Characterizing the Mechanical Performance of Laser Welded Lap Transverse Fillet Joints of Thick AISI 316L Stainless Steel

**Raghad A. Al-Aloosi** [a]*, **Furat I. Hussein** [b], **Ahmed R. Alhamaoy** [c], **Muhannad A. Obeidi** [d]

[a] Automated Manufacturing Department, Al-Khwarizmi College of Engineering, University of Baghdad, Baghdad, 10071 Iraq.
[b] Mechatronics Engineering Department, Al-Khwarizmi College of Engineering, University of Baghdad, Baghdad, 10071 Iraq.
[c] Department of Laser and Optoelectronic Engineering, College of Engineering, Al-Nahrain University, Baghdad, Iraq.
[d] I-Form Advanced Manufacturing Research Centre, Dublin City University, Ireland.

**Keywords:**
Austenitic 316L stainless; Laser welding; Mechanical performance; Single and double fillet; Tensile testing; Bending testing.

**Highlights:**

- Laser welding of stainless steel 316L joints was experimented.
- Lap welded joints were characterized through a series of tests including tensile, bending, and hardness.
- Manipulating process parameters have a significant effect on the lap welded joints by laser.
- Weld zones free of porosity or cracks are a requirement for optimal welding.

ARTICLE INFO

*Article history:*

| | |
|---|---|
| Received | 29 Sep. 2023 |
| Received in revised form | 03 June 2024 |
| Accepted | 07 Sep. 2024 |
| Final Proofreading | 13 June 2025 |
| Available online | 18 Aug. 2025 |



**Citation:** Al-Aloosi RA, Hussein FI, Alhamaoy AR, Obeidi MA. **Characterizing the Mechanical Performance of Laser Welded Lap Transverse Fillet Joints of Thick AISI 316L Stainless Steel**. *Tikrit Journal of Engineering Sciences* 2025; **32**(3): 1739.
http://doi.org/10.25130/tjes.32.3.17

*Corresponding author:
**Raghad A. Al-Aloosi**
Automated Manufacturing Department, Al-Khwarizmi College of Engineering, University of Baghdad, Baghdad, 10071 Iraq.

**Abstract**: Fillet and double fillet welding are extensively used in numerous structural applications around the globe. Laser welding technology has achieved great appeal due to its superior quality, accuracy, speed, adaptability, and versatility. The present investigation examines two modes of transverse welding, namely single fillet and double fillet weldments, on austenitic 316L stainless steel sheets with a thickness of 3 mm. The welding was performed using a $CO_2$ laser, eliminating the need for filler material. The mechanical performance was evaluated through tensile shear, bending, and micro-hardness tests. The investigation revealed a notable correlation between the laser power and scanning speed as working parameters on the joint's strength. The analytical results indicated that the optimal working parameters were a laser power of 2.75 kW and a scanning speed of 5 mm/s. These parameters resulted in a yield strength of 186.98 MPa and 275.91 MPa for the single fillet joints and double fillet joints, respectively. The three-point bending test showed flexural yield strength of 328.73 MPa and 893.57 MPa for the single and double fillets, respectively. The area under the flexural stress-strain curve reveals high ductility for both joining modes, represented by the broad area under the curve. This refers to the energy consumed per unit volume required to bend and deform the weldment until fracture.

# تقييم الأداء الميكانيكي للوصلات التراكبية الملحومة بالليزر لسبائك الفولاذ المقاوم للصدأ السميك AISI 316L

**رغد احمد الالوسي[1]، فرات ابراهيم حسين[2]، احمد رياض الحموي[3]، مهند أحمد عبيدي[4]**

[1] قسم هندسة التصنيع المؤتمت / كلية الهندسة الخوارزمي / جامعة بغداد / بغداد - العراق.

[2] قسم هندسة الميكاترونكس / كلية الهندسة الخوارزمي / جامعة بغداد / بغداد - العراق.

[3] قسم هندسة الليزر والالكترونيات البصرية / كلية الهندسة / جامعة النهرين / بغداد - العراق.

[4] مركز آي فورم لابحاث عمليات التصنيع المتقدمة / جامعة دبلن / دبلن – ايرلندا.

**الخلاصة**

يتم استخدام وصلات اللحام المفردة والمزدوجة على نطاق واسع في العديد من تطبيقات لحام الهياكل حول العالم. لقد حققت تقنية اللحام بالليزر جاذبية كبيرة بسبب جودتها الفائقة ودقتها وسرعتها وقابليتها على الموائمة بالاضافة الى تعدد الاستخدامات. في العمل الحالي، تم تحقيق نمطين من اللحام العرضي للوصلات المفردة والمزدوجة لصفائح الفولاذ المقاوم للصدأ الأوستينايتي 316L بسماكة 3 mm بواسطة ليزر ثاني أوكسيد الكربون (CO2) وبدون الاستعانة بمعدن حشو. تم فحص الأداء الميكانيكي من خلال اختبارات الشد والانحناء والصلادة الدقيقة. أظهرت نتائج البحث التأثير البارز لمعلمات عملية اللحام بالليزر وهي قدرة شعاع الليزر (*P*) وسرعة المسح (*v*)على قوة وصلات اللحام. تمييزت معلمات العمل المثالية، والتي تم تسجيلها كقدرة شعاع الليزر والتي تبلغ 2.75 kW وسرعة مسح تبلغ 5 mm/s، من خلال نتائج الاختبارات المتمثلة في مقاومة الخضوع والتي تبلغ 186.98 MPa للوصلات التراكبية المفردة. وبالمثل، سجلت الوصلات التراكبية المزدوجة مقاومة خضوع قدرها 275.91 MPa. اظهر اختبار الانحناء ثلاثي النقاط مقاومة انحناء تبلغ 328.73 MPa و 893.57 للوصلات المفردة والمزدوجة على التوالي. كشفت المساحة تحت منحنى الإجهاد والانفعال لاختبار الانحناء مطيلية عالية لكلا النوعين من الوصلات والمتمثلة في المساحة الكبيرة أسفل المنحنى. يمكن أن يترجم هذا إلى كمية الطاقة المستهلكة لكل وحدة حجم مطلوبة لتشويه اللحام قبل الكسر.

**الكلمات الدالة:** الفولاذ الأوستينايتي ٣١٦L، اللحام بالليزر، الأداء الميكانيكي، وصلات مفردة ومزدوجة، اختبار الشد، اختبار الانحناء.

## 1.INTRODUCTION

Around 1970, the development of multi-kilowatt lasers [1] expanded the horizons of thick-scope metal welding, offering higher quality, more precision, less processing time and lower costs for various applications [2]. Laser welding is widely used today as a replacement for conventional welding for joining steel alloy plates with a thickness of up to 10 mm [3]. Some traditional welding procedures require preheating to locally distort and soften the weld metal. The laser, as a welding tool, has addressed such problems, enhanced the quality of the welds, and yielded higher strength welds with less distortion and a narrower heat-affected zone (HAZ) [4]. The fundamental laser weld is the conduction mode, where most of the absorbed laser energy at the surface transfers through conduction and convection, forming a limited-depth weld pool of less than a few millimeters [5]. Welding in conduction mode can be achieved with a maximum power density of $10^5$ W/cm$^2$ [6]. Keyhole mode welding is realized when the laser beam has a sufficient power density (more than $10^6$ W/cm$^2$) and a certain slow speed that causes metal boiling and evaporation, a high-pressure vapor gas tunnel initiates along the weld depth, known as a keyhole [5]. Absorption of the laser beam inside the keyhole is achieved via two mechanisms: Fresnel and inverse bremsstrahlung. The latter has a major contribution in leading to laser absorption and achieving high welding efficiency [7]. In other words, the keyhole zone acts like a conduit that efficiently supplies the material with the required energy to cause welding [8]. Unlike conduction laser welding mode, keyhole weldments exhibit a higher aspect ratio and much lower distortion [9]. The energy supplied from a laser beam to the target should be well controlled to achieve optimum welding and avoid thermal effects [10]. Excessive heating, however, leads to a wider HAZ and a higher possibility of inducing porosity and microcracks, resulting in the degradation of welding strength and quality [11]. Laser welding with a pulsed laser differs from welding with a continuous wave (CW) laser in terms of the number of parameters that influence the weld geometry and microstructure. CW welding requires control over fewer parameters than pulsed laser, such as power density, scanning speed, focal position, angle of incidence [12], and beam spinning trajectory [13]. CW laser beams are preferable in welding types of metals that are insensitive to excess heat as well as for achieving deeper welding penetration [14]. In welding with a CW laser of defined spot size and shape, two fundamental operating parameters are essential in determining the geometry and dimensions of the weld zone: power density and scanning speed. In addition, it may be influenced by the employed shielding gas parameters during welding [15]. The interaction of the laser beams with the material has some effects on the welding process in CW mode. When a laser beam scans at constant speed along a given line, each spot on the surface is exposed to an equal period, called the interaction time, and thus takes the same amount of energy. For a certain value of power density, which is defined as the beam power over spot area, the interaction time for a given beam moving at a certain speed can be expressed as [16]:

$$t_i = \frac{d}{v} \quad (1)$$

where $t_i$ is the interaction time (s), $d$ is the beam diameter (m), and $v$ is the scanning speed (m/s).

The interaction time and laser output power play a significant role in defining the total energy poured on the target through the irradiated zone, which is expressed by the term specific point energy [16]:

$$E_s = P_d\, t_i\, A_s = P\, t_i \qquad (2)$$

where $E_s$ is the specific point energy (J), $P_d$ is the power density (W/$cm^2$), $A_s$ is the laser spot area on the target ($cm^2$), and $P$ is the laser power (W). Suder and Williams suggested that the power density and specific energy are responsible for the weld penetration depth, while the weld width is correlated with the interaction time, which can also be expressed in terms of scanning speed [17]. The power factor integrates the power density and beam diameter to evaluate the penetration depth [18]:

$$P_f = P_d\, d = \frac{P}{d} \qquad (3)$$

where $P_f$ is the power factor (W/m).

The American Welding Society (AWS) has identified the five most common types of weldments, namely butt, Tee, lap, corner, and edge joints [19]. In lap, Tee, and corner configurations, the fillet weld is utilized to fill the meeting borders of joint plates. Lap joints, as well as Tee joints, can be welded in various forms: single or double fillet (Fig. 1), continuous or intermittent, and with a single weld pass or multiple weld passes [20]. Lap fillet joints, which are featured by their good strength and fewer preparation requirements are commonly utilized in the applications of metallic structures welding. They show some difficulties in welding with a consistent degree of consistency due to the challenges of achieving the correct weld geometry in terms of the required leg lengths, penetration depth, or throat thickness [21]. The design challenges in lap joints lie in overcoming the non-uniform stress distribution and eccentricity [22]. In many applications, double lap weldments without deep penetration are demanded to increase strength and avoid eccentricity, mismatching, and shear in only one direction under loading [23].

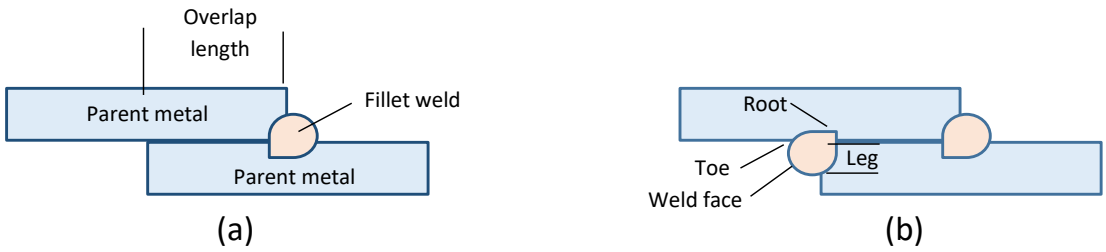


**Fig. 1** Lap Fillet Weldments: (a) Single Fillet-Single Pass, (b) Double Fillet-Single Pass.

Many researchers have investigated fillet lap laser welding. Ishak and Salleh [24] studied laser welding of thin AZ31B Magnesium alloy sheets in a double fillet lap joint using a low-power pulsed fiber laser, they investigated the effects of pulse energy and scanning speed on the joint strength, joint appearance and formed defects. Tawfiq et al. [25] employed a pulsed Nd:YAG laser to apply overlap spot welding for ferrous alloys. The study focused on examining the optimal parameters that result in the most significant joint strength through experimental and computer evaluation. Roos and Schmidt [26] applied an overlap configuration remote laser welding for zinc-coated steel sheets using a Yb:YAG fiber laser. They investigated the influence of laser welding operating parameters on the process stability and weld quality. In addition, they discussed the effect of beam positioning on joint strength and the density of emitted spatters. Khan et al. [27] utilized a CW Nd:YAG laser to perform circular welding on two types of stainless steel tubes, namely AISI 304L and AISI 430 (austenitic/ferritic). The influence of various parameters, such as laser power, scanning speed, incident angle, and focal position, on joint strength, weld geometry, and the formed microstructure, was investigated. Unt and Salminen [28] applied fillet laser welding to a T-type configuration of thick, low-alloy structural steel sheets AH36 using a high-power fiber laser. The influence of each variable at a time welding speed, laser power, focus position, and beam angle, on the heat input and, accordingly, its effects on weld bead geometry are studied. The present work is devoted to applying effective keyhole laser welding for fillet lap joints of thick 316L stainless plates using a CW CO2 laser beam without filler material to investigate the effective working parameters that yield the best mechanical performance. The optimum set of working parameters is selected to achieve the best combination of mechanical properties and no distortion. The main source of distortion can be attributed to the absence of any filler and additive materials. Also, poorly adjusted parameters values can result in over-melting and the formation of holes at extremely high laser power levels and/or slow scanning speeds, and vice versa.

## 2.EXPERIMENTAL SETUP

### *2.1.Sheets Preparation*

Stainless steel 316L is a type of austenitic stainless steel series characterized by its good mechanical properties [29]. Due to the addition

of Cr 18% and 8% Ni, this alloy acquired exceptional corrosion/oxidation resistance, moderate tensile strength, better formability, and good weldability. These properties render these alloys highly demanded in the chemical and petrochemical industries at high temperatures [30], power plants components [31], medical-surgical, and transportation applications [32]. Commercial stainless steel alloy sample sheets of 3 mm thickness were used in single and double-fillet single-pass overlap laser welding. The standard test method, ASTM E108, for the analysis of the alloy by spark atomic emission spectrometry technique, reveals that the selected alloy is cold-rolled, annealed austenitic AISI 316L stainless steel UNS S31603. Table 1 presents the chemical composition of the employed alloy. A tensile test was conducted on a sample of the aforementioned alloy to investigate its mechanical behavior under loading. The test revealed acceptable convergence with the mechanical properties presented in Table 2 for the alloy, as per the ASM standards. Each sample was cut to square edges and prepared to dimensions of 17 mm × 80 mm. Before the welding process, the samples were polished using abrasive papers to remove the edge burrs produced by cutting and then cleaned with acetone to remove any possible contaminants.

**Table 1** The Chemical Composition of AISI 316L Alloy (in Weight %) [33].

| C | Mn | Si | P | Cr | Ni | Mo | S | Cu | Fe |
|---|---|---|---|---|---|---|---|---|---|
| 0.0356 | 1.76 | 0.509 | 0.0467 | 16.80 | 10.40 | 1.94 | 0.0066 | 0.345 | bal. |

**Table 2** Some Mechanical Properties of AISI 316L Alloy [33].

| Young's Modulus (GPa) | Yield Strength (MPa) | Tensile Strength (MPa) | Elongation (%) | Hardness |
|---|---|---|---|---|
| 200 | 310 | 595 | 51 | HB 82<br>HR 79 |

### *2.2.Experimental Setup*

Each pair of cut sheets for the tensile test was placed in a clamping device and fixtures that ensured a 35 mm overlap configuration and maintained adequate contact at the weld joint (ideally with zero gaps). A CW $CO_2$ laser of 4 kW maximum power and a wavelength of 10.6 µm (Trumpf TLF 4000 Turbo) was used to achieve welding. Keyhole laser welding was conducted by focusing the laser beam on the front side edge of the upper sheet with a spot radius of about 0.15 mm. Figure 2 shows a schematic diagram of a single-sided fillet lap laser welding process, which is conducted in a single pass. To shield the delivery optics from the generated plasma and splatter, the laser head was adjusted to a position where the incidence of the laser beam on the target was inclined at two angles, i.e., a backward angle of 85° and a sideward tilt angle of 75°. The focal distance was maintained g at 200 mm between the workpiece and the laser head during welding. A coaxial gas nozzle was installed on the laser head, through which argon assist gas was pumped at a flow rate of 18 *l*/min. The objective is to build a tent of argon gas over the interaction zone to shield the workpiece against oxidation and protect the optical elements. Double fillet lap welding was achieved by flipping a single fillet-welded sample and welding the other unwelded side.

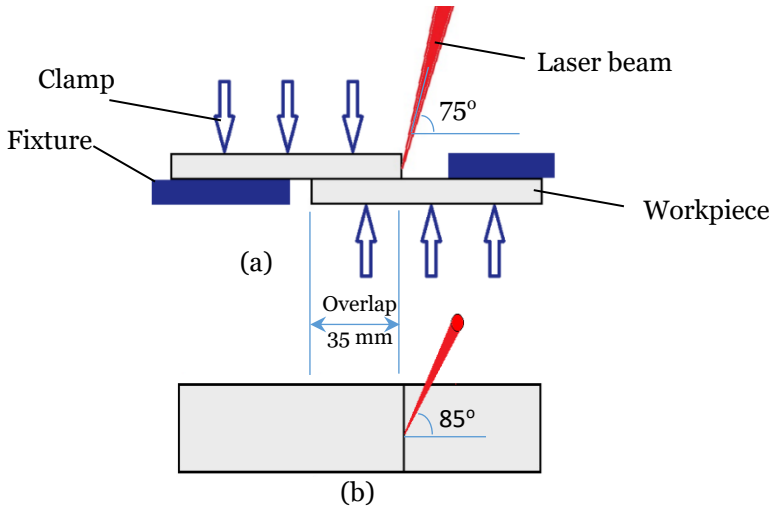


**Fig. 2** Single Fillet Lap Laser Welding Setup (not in Scale): (a) Side View, (b) Top View.

### *2.3.Processing Parameters*

The parameters of laser power and scanning speed were chosen as working parameters in keyhole welding to verify the optimum welding conditions, as represented by joint strength and bead appearance. For each scanning speed value, the laser power was varied by specific values as follows: the lower limit of laser power required to fuse the front side of the upper sheet and bridge with the lower sheet. Sufficient laser power is required to achieve maximum penetration in the lower sheet without causing sample bending or distortion resulting from thermal stresses, where zero deflection is unavoidable. Accordingly, the laser power was varied from 1.5 to 2.5 kW, and the scanning speed varied from 3 to 5 mm/s. The investigation was performed in a series of welded samples according to a set of parameters listed in Table 3, which displays both experimental and estimated values.

**Table 3** The Experimental and Estimated Parameters for Single and Double Fillet Welding.

| Sample Groups | | $P$ (kW) | $v$ (mm/s) | $t_i$ (s) | $E_s$ (J) | $P_f$ (kW/mm) |
|---|---|---|---|---|---|---|
| Single fillet | Double fillet | | | | | |
| S1 | D1 | 2.25 | 5 | 0.06 | 0.135 | 7.5 |
| S2 | D2 | 2.75 | 5 | 0.06 | 0.165 | 9.167 |
| S3 | D3 | 3.25 | 5 | 0.06 | 0.195 | 10.833 |
| S4 | D4 | 2.75 | 3 | 0.1 | 0.275 | 9.167 |
| S5 | D5 | 2.75 | 6 | 0.05 | 0.1375 | 9.167 |
| S6 | D6 | 2.75 | 8 | 0.0375 | 0.10312 | 9.167 |

### *2.4.Inspection and Characterization of Samples*

The mechanical performance of the welded joints was tested through many mechanical tests. A tensile shear test was conducted to evaluate the joint strength using a universal testing machine (Testometric AX M500-25kN, UK) at room temperature with a ram speed of 5 mm/min. The bending test is beneficial for evaluating the ductility and soundness of welded joints [34], which can degrade due to the presence of discontinuities, porosity, or internal inclusions [35]. Using the same testing device, a three-point bending test was performed according to ASTM E290–14 for bend testing of materials to assess ductility [36]. In the bending test of single fillet samples, the load was applied on the unwelded side of the sample (typically in a press). The test was conducted at room temperature, and the load was applied to the middle of the sample at a speed of 5 mm/min for each sample. Vickers microhardness apparatus (Q-Time, China) was utilized to evaluate the microhardness profile across the weld side section. As shown in Fig. 3, the test was performed at eleven points along a straight line that starts from the base metal, passes through the HAZ, fusion zone, and ends at the base metal on the other side. The section surface was cleaned and polished before the test was applied. The indenter was loaded with a load of 4.903 N for a dwell time of 10 s as dwell time. The microstructural changes in the joining zone were examined using an optical microscope from Keyence 2000. To enhance the visual contrast of the grain boundaries, the welded fillets were polished in the cross-sectional direction using Buehler Motopol 2000 polisher. The polishing process was conducted by applying successive grades of silicon carbide paper of 400, 600, 800, 1200, 2500, and 4000. Final polishing was conducted using an Oextmet cloth with diamond and alumina suspensions of 6, 3, 1, and 0.05 microns particle size sequentially. Each polishing grade was applied for 5 to 8 minutes with rotational speed of 250 rpm. Glyceregia etchant was used to reveal the grain boundaries and orientation. Glyceregia, composed of 20 ml of nitric acid, 30 ml of hydrochloric acid, and 20 ml of glycerol, was applied for 3 to 5 seconds by swabbing the polished area with a cotton cloth. The evaluation of the optimum samples was conducted to observe the microstructural changes resulting from the welding process.

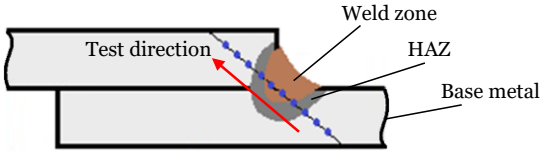


**Fig. 3** Evaluating the Microhardness Profile Line Across the Joint Side Section Passing Through the Base Metal HAZ and Fusion Zone (not in Scale).

## 3.RESULTS AND DISCUSSION

### *3.1.Tensile Test*

The obtained results of shear tensile tests for all produced samples are presented as follows:

**a)** Single fillet samples (S-group): Figure 4 shows the stress-strain curve obtained for each optimum sample in the S-group. The S2 sample, produced with operation parameters of 2.75 kW laser power and a scanning speed of 5 mm/s, was considered the optimum result among the other samples. Figure 5 (a) shows how S2 breaks under loading. It was broken at the HAZ recording yield strength of 186.98 MPa and failure strain of 13.66%. During loading, the S samples show joint rotation due to the diffraction of the applied load at the samples ends. The majority of samples exhibited fracture, with crack propagation occurring at the interface zone between the base metal and HAZ. The optimum

samples, S2, combine relatively high yield strength, high ultimate tensile strength (UTS), and a large amount of energy absorption during loading and plastic deformation. The latter is represented by the weaker frailer strain of 13.66%, as indicated in Table 4. The Visual inspection of one of the failed samples reveals extreme ductile stretching in the weld zone prior to fracture, as illustrated in Fig. 5 (a).

**b)** Double Fillet Samples (D-group): Fig. 5 (b) shows that under loading D2 samples showed high stability until the fracture occurs. Fracture of the D2 samples occurred at the base metal side, without noticeable deformation or stretching, for both weld beads of the sample. Figure 6 displays the stress-strain behavior for the double fillet sample D-group. By analogy with the S-group, the stress-strain curve indicates that D2 was the optimal sample in terms of combining good mechanical properties with better ductility. S2 and D2 sample groups shared the same operating parameters. The D2 sample recorded a yield stress of 275.91 MPa and a failure strain of 37.6%.

Table 4 illustrates the mechanical properties obtained from the tensile test for the optimum values of both single and double S2 and D2 samples, respectively.

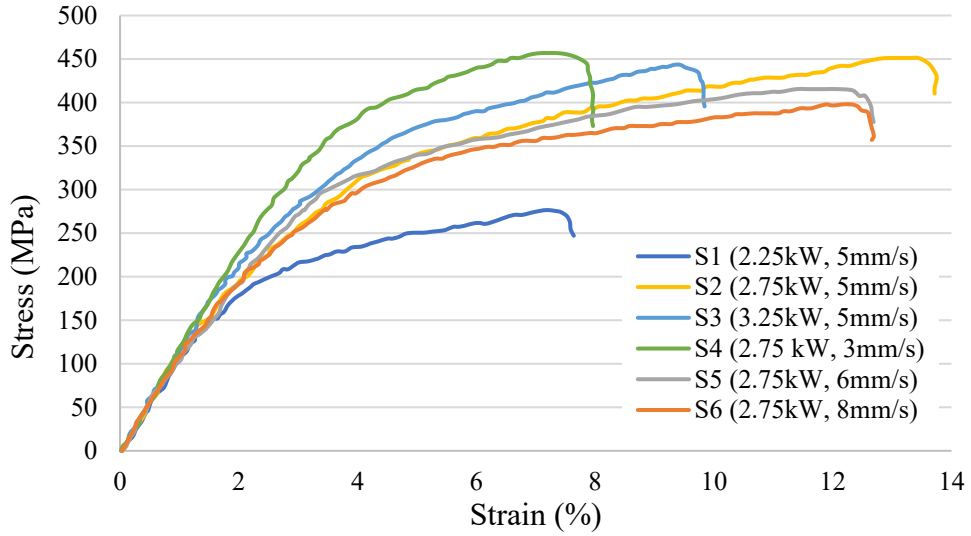


**Fig. 4** Tensile Test Results for Single Fillet Joints (S-Group).

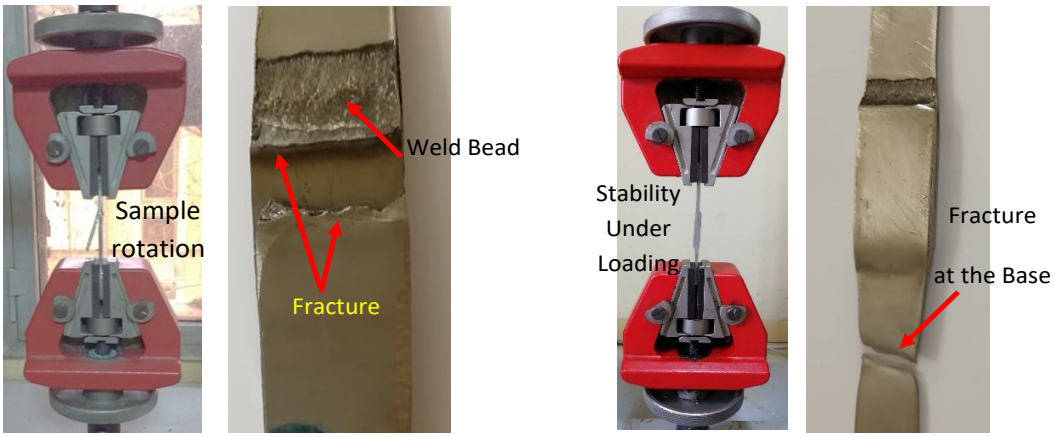


**Fig. 5** (a) Single Fillet Sample During Loading and Fractured Sample, (b) Double Fillet Sample During Loading and Fractured Sample.

**Table 4** The Mechanical Properties for the Produced Fillet Single and Double Joints for Single and Double Fillet Samples Welded at Operating Conditions of 2.75 kW Power and 5 mm/s Scanning Speed.

| Property / Samples | Yield Stress (MPa) | Yield Strain (%) | UTS (MPa) | Failure Strain (%) |
|---|---|---|---|---|
| Single Fillet (S) | 186.98 | 3.75 | 435 | 13.66 |
| Double Fillet (D) | 275.91 | 5.4 | 495 | 37.6 |

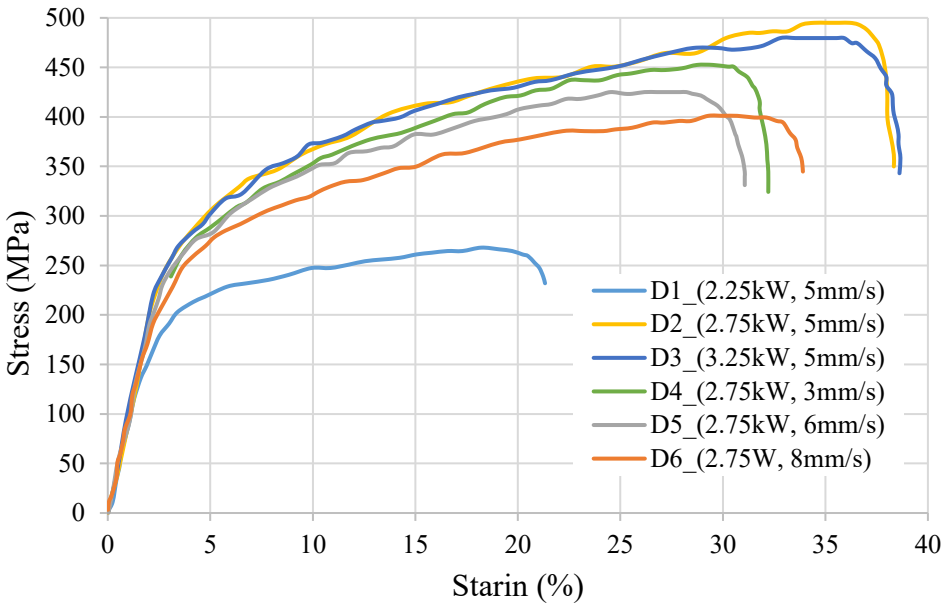


**Fig. 6** Tensile Test Results for Double Fillet Joints (D-Group).

### *3.2.Effect of Interaction Parameters on the Weld Characteristics*

At a fixed laser spot diameter, variations in laser power and scanning speed resulted in different interaction parameters between the laser and the target. In this section, the optimum weld was correlated with suitable weld dimensions (depth and width) that are free of defects due to excessive heating, which contributes to its degradation. Figure 7 reveals that the S2 and D2 samples showed the best weld dimensions, free from heating defects, at the combination of interaction parameters values of Es=0.165 J, ti=0.06 s, and Pf= 9.17 kW/mm. Lower values of interaction parameters result in S1 and D2 samples showing significant retrogression in strength and ductility, which may be related to insufficient weld depth and width. Higher values than the optimum conditions (S3 to S6 and D3 to D6) displayed a gradual decrease in mechanical behavior, indicating the formation of weld defects due to excessive heating.

### *3.3.Effect of Weld Overlap on Flexural Strength*

The bending test delivers a measure of the flexible behavior of the welded joints. It is well known that when a material is subjected to a bending load, tensile, and compression stresses generate in convex and concave sides, respectively [37]. Three samples were welded under optimum welding conditions, determined from the tensile test, at a power of 2.75 kW and a scanning speed of 5 mm/s for the S2 and D2 samples with three different overlap lengths: 75, 100, and 125 mm. Each test started and continued until the specimen lost its capacity to carry the applied load and took the U-shape without observed fracture. Figure 8 shows the flexural stress-strain test for the single and double fillet samples. The schematic diagram for the bending test is clarified in Fig. 8 (a) for a double fillet sample. A transverse fillet weld means the weld seam is perpendicular to the applied force during service. When the double fillet sample is subjected to a three-point bending test, the neutral axis is at the contact surface of the two overlapped surfaces. Figure 8 (b) compares S and D fillet samples under bending loading. Maximum bending stress/strain recorded values of 328.73 MPa / 58.32 % and 893.57 MPa / 29.34 % for the single and double weldments, respectively. However, the flexure stress-strain curve shows good strain and a wide area under the curve before failure. It reflects the good ductility and a large amount of energy required to cause failure. The good ductility was deduced from the bend angles of approximately 90° for the S samples and less than 90° for the D samples. As the load pushed the sample to bend from one side, no cracks were noticed on the outer side before failure, which occurred at the HAZ. In most cases, the welded joints under bending tests are most sensitive to defects adjacent to the weld zone [35]. Compared to the single fillet mode, the double fillet joints exhibited more strength and better ductility. As a matter of fact, the test of a single fillet joint was quite similar to the behavior of a single plate under the bending load due to the departure of plates during the bending test. By comparing both joints, double fillet joints showed a higher withstand due to their resistance to the slipping of the overlapped plates under the effect of variant-induced stresses in the upper and lower plates. Table 5 illustrates the mechanical properties conducted from the bending test for the optimum values of both S and D samples.

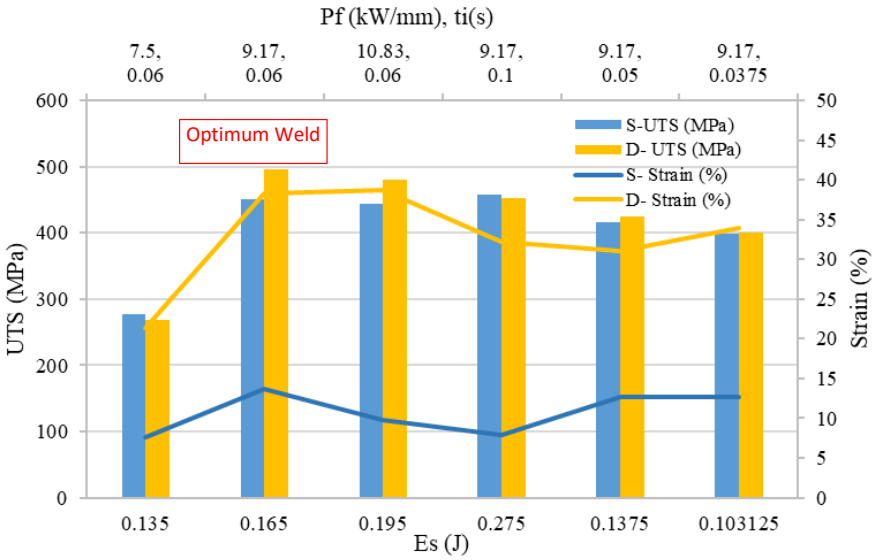


**Fig. 7** The Optimum Weld Achieved at Es= 0.156 (J), Pf= 9.17 kW/mm, and ti= 0.06s.

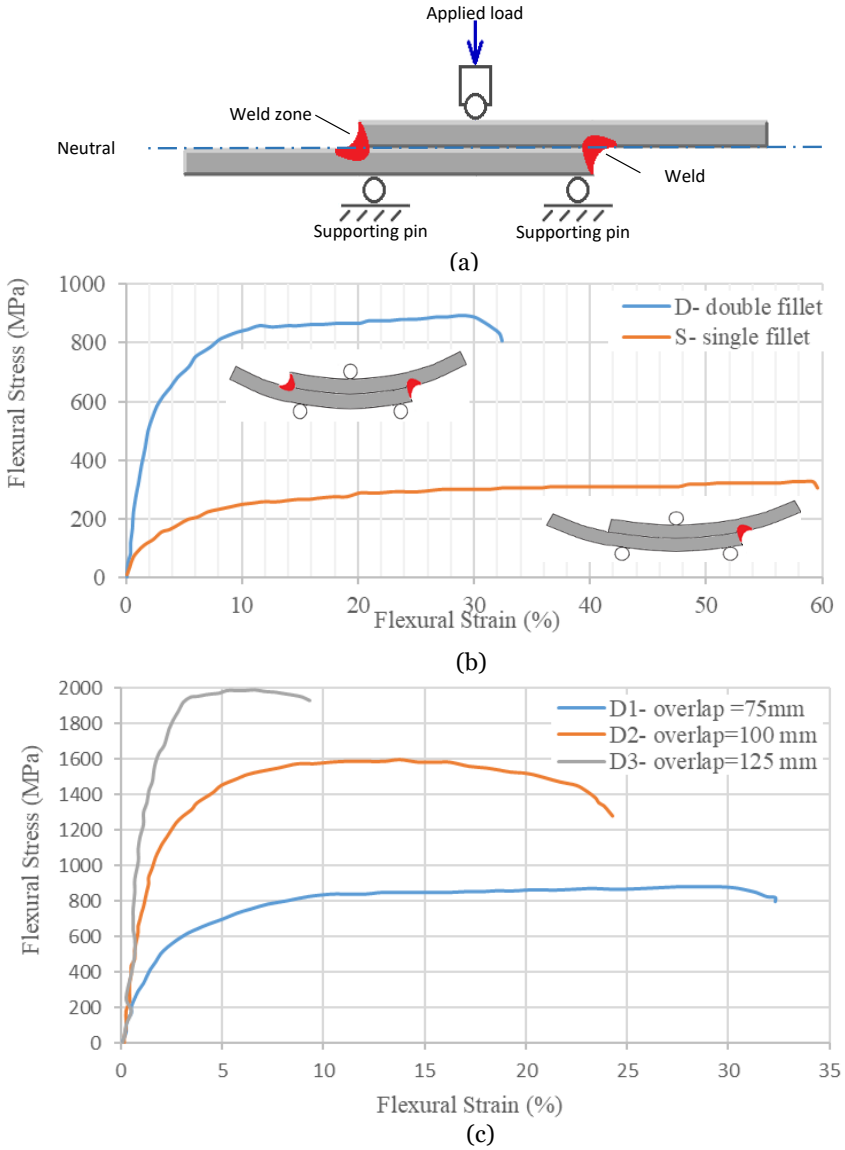


**Fig. 8** Bending Test for Single and Double Fillet Samples Welded at Operating Conditions of 2.75 kW Power and 5 mm/s Scanning Speed: (a) a Schematic Diagram for the Setup of Double Fillet Sample, (b) Flexural Stress-Strain Curve for the Optimum Single and Double Fillet at the Overlap of 35 mm, and (c) Effect of Overlap Length on the Strength and Strain of Double Fillet Samples.

**Table 5** The Mechanical Properties Obtained from the Bending Test for Single Fillet S2 and Double Fillet D2 Joints at 35 mm Overlap.

| Property / Samples | Flexural Modulus of Elasticity (MPa) | Flexural Yield Stress (MPa) | Flexural Yield Strain (%) | Flexural UTS (MPa) | Failure Strain (%) |
|---|---|---|---|---|---|
| Single Fillet (S) | 90 | 125 | 1.75 | 328.73 | 57 |
| Double Fillet (D) | 140 | 610 | 3 | 893.57 | 32 |

Figure 9 shows the shear force and bending moment diagrams at the ultimate loading point prior to the onset of failure. In double fillet samples, the neutral axis was located at the contact surface between the two overlapping plates. The upper plate and weld zone were subjected to compressive stresses. Conversely, the lower surface and weld experienced tensile stresses.

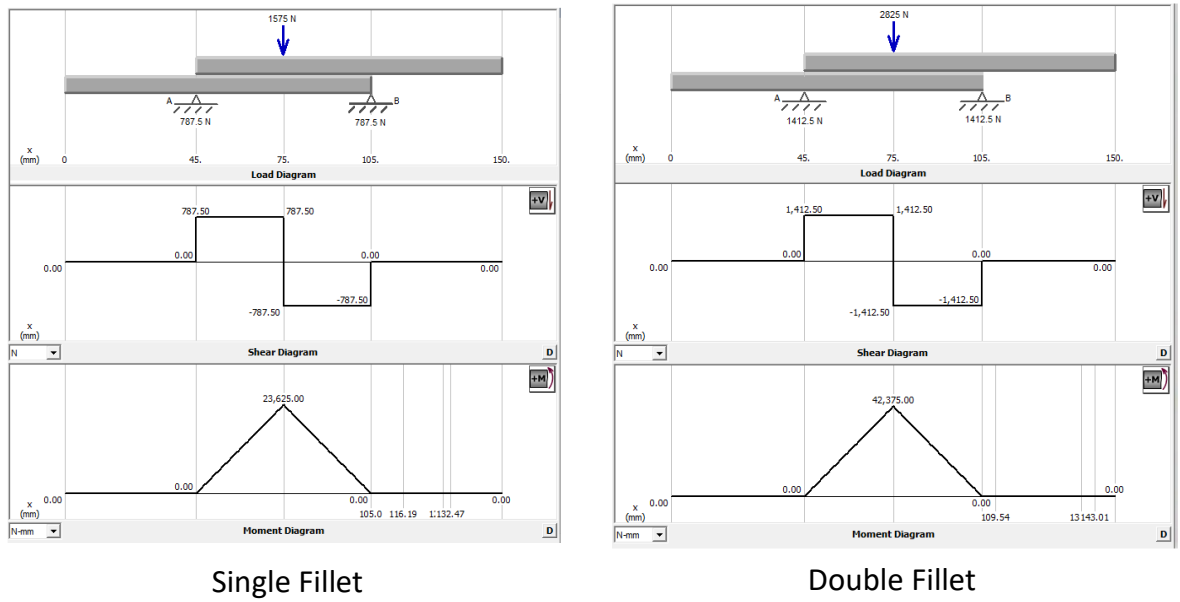


Single Fillet Double Fillet

**Fig. 9** Shear Force and Bending Moment Diagrams for Single and Double Fillet Joints (Plotted by MD Solids Software 4.1.0).

### *3.4.Hardness Test*

Upon analyzing the hardness profile along the specified inclined path in Fig. 2, it is observed to take the M shape, as shown in Fig. 8. The order of the most significant values of microhardness is for the HAZ, followed by the weld zone and finally the base metal, which may be attributed to the fact that the HAZ was adjacent to the cold block of the bulk material; therefore, it was certainly subjected to a somewhat greater cooling rate compared with the weld zone, resulting in the formation of the martensite hard phase [38]. A thermal treatment that provides tempering of the martensite in the weld zone and HAZ may lessen the range of hardness values throughout the joint [39].

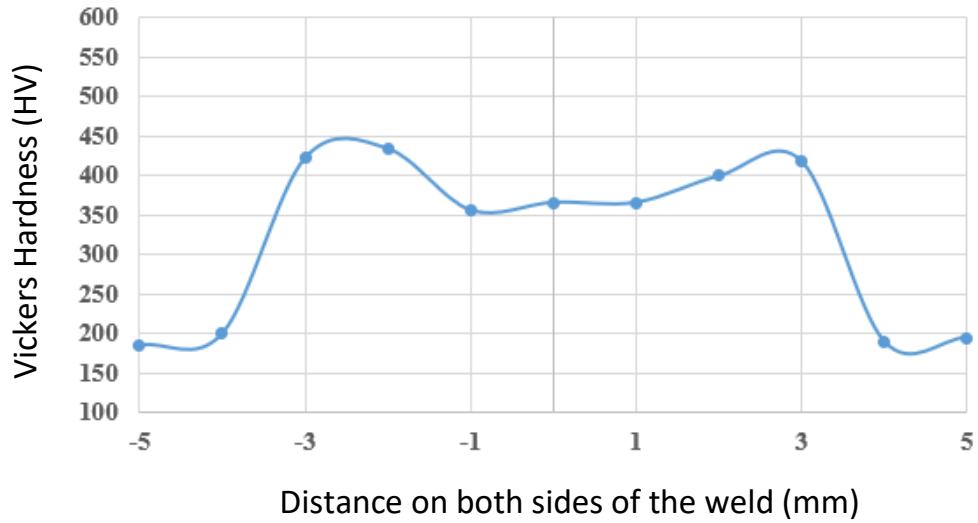


**Fig. 10** Vickers Microhardness Profile Line Across the Joint Section Passing Through the Base Metal HAZ and Fusion Zone.

### *3.5.Appearance and Microstructure*

A compromise between maximum weld penetration and minimum HAZ in lap fillet joints is required in the case of structural applications of welded parts. This compromise involves adjusting the operating parameters to achieve a more optimal weldment profile as well as minimizing the side effects of HAZ, which in turn reflects the optimum mechanical behavior under loading. The laser power and scanning speed ranges were adjusted until a good seam was achieved, as represented by the S2 and D2 sample groups shown in Fig. 11 (a). Based on visual inspection, the joint showed a concave bead face with no undercuts and negligible distortions due to thermal effects (Fig. 11 (b)). Employing higher laser power or lower scanning speed than that of the mentioned optimum conditions may achieve full penetration; however, it will be accompanied by excessive heating and thermal damages, where the S and D order of the samples from 3 to 6 exhibited such effects. In addition, the bad thermal effect results in material loss, burns on the surface of the back side of the weldment, and thermal deflection, as shown in Figs. 11 (c) and (d). The analysis of the microstructure for a fillet joint welded under optimal parameters reveals a regular, free of abnormalities and symmetrical fusion zone, as shown in the optical microscope images in Fig. 12 (a). The images do not indicate the presence of cracks or porosity in the samples. Higher magnification revealed a very limited width and tiny grain size, compared to the base metal, for the HAZ, as shown in Fig. 12 (b). The HAZ was constructed of both fusion zone and base metal in a random arrangement. It revealed mixed and extended zones of coarse and fine grains, which had different microstructures and sets of mechanical properties, hence diminishing the mechanical performance of the welded joint [40].

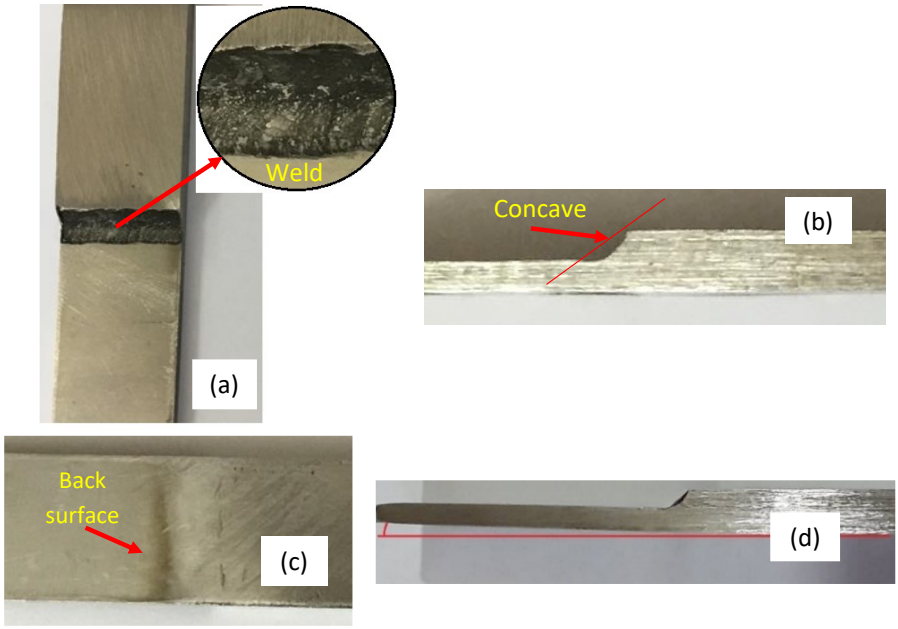


**Fig. 11** (a) The Weld Bead of S2 Sample was Achieved with the Optimum Conditions of 2.75 kW Laser Power and a Scanning Speed of 5 mm/s, (b) Joint Features for the Optimum Obtained Samples S2 or D2, (c) Back Surface Burning at the Weld Bead for S3 Sample Due to Excessive Heating, and (d) Distortion in the S3 Welded Sample Due to Thermal Stresses Resulted from Excessive Heating.

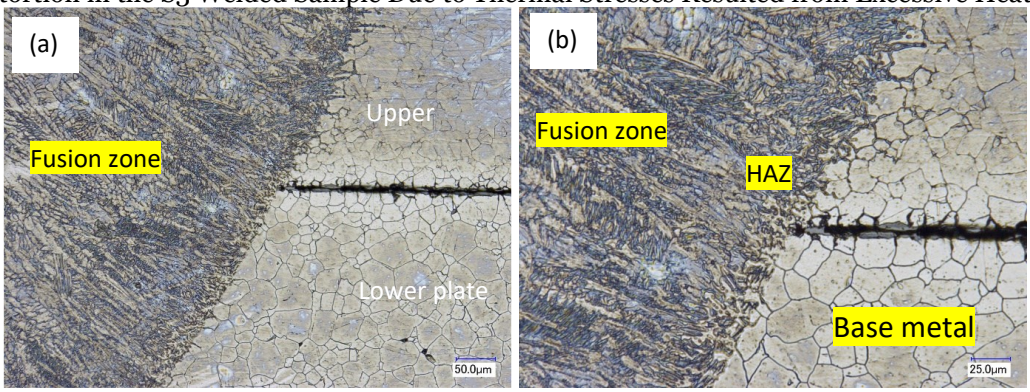


**Fig. 12** Optical Micrographs of the Microstructure for a Sample (S2) Welded with the Optimum Welding Conditions: (a) The Joint Welded Sheets and Fusion Zone, (b) A Magnified Zone Exhibiting the Fusion Zone, HAZ, and the Base Metal.

### *3.6.The Impact of Laser Power and Scanning Speed*

The above results showed the significant impact of laser power and scanning speed on creating flawless, pore-free, and ideal microstructures, resulting in optimal mechanical performance of the weldments. Increasing the laser power results in a wider weld pool and deeper penetration. However, this behavior is associated with a specific power threshold, above which there is excessive melting, increasing presence of flaws, porosity, and oxidation, ultimately diminishing the strength of the joint. The scanning speed and cooling rate are directly correlated as the laser beam traverses a certain region [41]. Higher scanning speed decreases the interaction time, which is directly related to the amount of heat transferred to the weldment, resulting in a narrower weld bead, reduced penetration depth, and incomplete fusion. Furthermore, the increase in scanning speeds leads to higher cooling rates throughout the welding process. Conversely, at lower speeds, the interaction time in a particular region extends longer, leading to a slower cooling rate and the formation of a cellular dendritic microstructure.

## 4.CONCLUSIONS

The mechanical performance and microstructure of AISI 316L alloy transverse lap laser welded joints were investigated. Single and double fillet welds were performed on 3 mm thick sheets. The following conclusions can be derived from this work:

- A maximum yield tensile strength of 186.98 MPa for single fillet and 275.91MPa for double fillet welded with 2.75 kW laser power and 5 mm/s traverse speed. On the contrary, the lowest strengths of 126.91 MPa and 136.31 MPa for single and double fillets, respectively, were achieved when the samples were welded at a power of 2.25 kW and a scanning speed of 5 mm/s.
- The maximum bending strength of 328.73 MPa for the single fillet and 893.57 MPa for the double fillet, along with the largest ductility, was achieved with the same welding parameters that yielded the largest tensile strength.
- The results showed that the optimum conditions were achieved with a moderate interaction time and specific point energy of 0.06 s and 0.16 J, respectively. The extreme values of the estimated parameters resulted in higher weld penetration accompanied by back surface burning and more distortion due to thermal stresses.
- In double fillet weld, the increase in the overlap value had a direct relationship with the weldment strength and an inverse relationship with the strain.
- The hardness profile across the weldment exhibited an M-shaped pattern, with fluctuations ranging from 350 to 360 HV. These values are significantly higher than the base metal hardness of 200 HV.
- No visual defects were noted on the weldment during the bending test, and the ductility of the welded specimens was acceptable.

## ACKNOWLEDGMENT

This study has emanated from research supported by the Automated Manufacturing Engineering Department and the Mechatronics Engineering Department, Al-Khwarizmi College of Engineering, University of Baghdad. Part of the experimental and characterization work was supported by a research grant from Science Foundation Ireland (SFI) under grant number 16/RC/3872 and is co-funded under the European Regional Development Fund.

## NOMENCLATURE

| | |
|---|---|
| $t_i$ | Interaction time, s |
| $d$ | Beam diameter, mm |
| $v$ | Scanning speed, m/s |
| $E_s$ | Specific point energy, J |
| Pd | Power density, W/cm$^2$ |
| $A_s$ | Laser spot area, mm$^2$ |
| $P$ | Laser power, W |
| $P_f$ | Power factor, W/m |

## REFERENCES

**[1]** Mazumder J. **Laser Welding: State of the Art Review.** *Journal of Metals* 1982; **34**(7):16-24.

**[2]** Unt A, Poutiainen I, Grünenwald S, Sokolov M, Salminen A. **High Power Fiber Laser Welding of Single Sided T-Joint on Shipbuilding Steel with Different Processing Setups.** *Applied Sciences* 2017; **7**(12):1276.

**[3]** Sirohi S, Pandey SM, Tiwari V, Bhatt D, Fydrych D, Pandey C. **Impact of Laser Beam Welding on Mechanical Behaviour of 2.25Cr-1Mo (P22) Steel.** *International Journal of Pressure Vessels and Piping* 2023; **201**:104867.

**[4]** Kumar A, Pandey C. **Autogenous Laser-Welded Dissimilar Joint of Ferritic/Martensitic P92 Steel and Inconel 617 Alloy: Mechanism, Microstructure, and Mechanical Properties.** *Archives of Civil and Mechanical Engineering* 2022; **22**(1):39.

**[5]** Guo C, Singh SC. **Handbook of Laser Technology and Applications.** 2nd ed. Boca Raton: CRC Press; 2021.

**[6]** Cheepu M, Kumar Reddy YA, Indumathi S, Venkateswarlu D. **Laser Welding of Dissimilar Alloys Between High Tensile Steel and Inconel Alloy for High Temperature Applications.**

*Advanced Materials and Processing Technology* 2022; **8**(2):1197-1208.

**[7]** Cheng Y, Jin X, Li S, Zeng L. **Fresnel Absorption and Inverse Bremsstrahlung Absorption in an Actual 3D Keyhole During Deep Penetration CO2 Laser Welding of Aluminum 6016.** *Optics and Laser Technology* 2012; **44**(5):1426-1436.

**[8]** Steen WM, Mazumder J. **Laser Material Processing.** London: Springer London; 2010.

**[9]** Ayoola WA, Suder WJ, Williams SW. **Parameters Controlling Weld Bead Profile in Conduction Laser Welding.** *Journal of Materials Processing Technology* 2017; **249**:522-530.

**[10]** Prabakaran MP, Kannan GR, Pandiyarajan R. **Effects of Welding Speed on Microstructure and Mechanical Properties of CO2 Laser Welded Dissimilar Butt Joints Between Low Carbon Steel and Austenitic Stainless Steel.** *Advanced Materials and Processing Technology* 2022; **8**(sup1):1-12.

**[11]** Indhu R, Divya S, Tak M, Soundarapandian S. **Microstructure Development in Pulsed Laser Welding of Dual Phase Steel to Aluminium Alloy.** *Procedia Manufacturing* 2018; **26**:495-502.

**[12]** Assuncao E, Williams S. **Comparison of Continuous Wave and Pulsed Wave Laser Welding Effects.** *Optics and Lasers in Engineering* 2013; **51**(6):674-680.

**[13]** Dawes C. **Laser Welding.** Woodhead Publishing Limited; 1992.

**[14]** Fuerschbach PW, Eisler GR. **Effect of Laser Spot Weld Energy and Duration on Melting and Absorption.** *Science and Technology of Welding and Joining* 2002; **7**(4):241-246.

**[15]** Coroado J, Ganguly S, Williams S, Suder W, Meco S, Pardal G. **Comparison of Continuous and Pulsed Wave Lasers in Keyhole Welding of Stainless-Steel to Aluminium.** *International Journal of Advanced Manufacturing Technology* 2022; **119**(1-2):367-387.

**[16]** Meco S, Cozzolino L, Ganguly S, Williams S, McPherson N. **Laser Welding of Steel to Aluminium: Thermal Modelling and Joint Strength Analysis.** *Journal of Materials Processing Technology* 2017; **247**:121-133.

**[17]** Suder WJ, Williams S. **Power Factor Model for Selection of Welding Parameters in CW Laser Welding.** *Optics and Laser Technology* 2014; **56**:223-229.

**[18]** Coroado J, Meco S, Williams S, Ganguly S, Suder W, Quintino L. **Fundamental Understanding of the Interaction of Continuous Wave Laser with Aluminium.** *International Journal of Advanced Manufacturing Technology* 2017; **93**(9-12):3165-3174.

**[19]** **Drawing Practices.** 2009; **1994**.

**[20]** Groover M. **Fundamentals of Modern Manufacturing Materials, Processes and Systems.** John Wiley & Sons; 2010:493.

**[21]** McCormac JC, Csernak SF. **Structural Steel Design.** 5th ed. 2006:1-738.

**[22]** Miller DKD. **Designing Welded Lap Joints Practical Ideas for the Design Professional.** 2001; **18**(3):3-5.

**[23]** Jeffus L. **Welding: Principles and Applications.** Cengage Learning; 2012:947.

**[24]** Ishak M, Salleh MNM. **Double Fillet Lap of Laser Welding of Thin Sheet AZ31B Mg Alloy.** *Journal of Physics: Conference Series* 2018; **1027**(1):12003.

**[25]** Tawfiq TA, Taha ZA, Furat, Hussein I, Shehab AA. **Spot Welding of Dissimilar Metals Using an Automated Nd:YAG Laser System.** *Iraqi Journal of Laser, Part A* 2012; **11**:1-5.

**[26]** Roos C, Schmidt M. **Remote Laser Welding of Zinc Coated Steel Sheets in an Edge Lap Configuration with Zero Gap.** *Physics Procedia* 2014; **56**:535-544.

**[27]** Khan MMA, Romoli L, Fiaschi M, Dini G, Sarri F. **Laser Beam Welding of Dissimilar Stainless Steels in a Fillet Joint Configuration.** *Journal of Materials Processing Technology* 2012; **212**(4):856-867.

**[28]** Unt A, Salminen A. **Effect of Welding Parameters and the Heat Input on Weld Bead Profile of Laser Welded T-Joint in Structural Steel.** *Journal of Laser Applications* 2015; **27**(S2).

**[29]** Wahab A, Khuder H, Ebraheam EJ. **Study the Factors Effecting on Welding Joint of Dissimilar Metals.** *Al-Khwarizmi Engineering Journal* 2011; **7**(1):76-81.

**[30]** Bhanu V, Gupta A, Pandey C. **Role of A-TIG Process in Joining of Martensitic and Austenitic Steels for Ultra-Supercritical Power Plants - A State of the Art Review.** *Nuclear Engineering and Technology* 2022; **54**(8):2755-2770.

**[31]** Dak G, Pandey C. **Study on Effect of Weld Groove Geometry on Mechanical Behavior and Residual**

**Stresses Variation in Dissimilar Welds of P92/SS304L Steel for USC Boilers.** *Archives of Civil and Mechanical Engineering* 2022; **22**(3): 140.

**[32]** Rajesh KVD, Shaik AM, Buddi T. **Wear and Corrosion Analysis on Maraging Steel MS1 and Stainless Steel 316L Developed by Direct Metal Laser Sintering Process.** *Advanced Materials and Processing Technology* 2022; **8**(sup3):1135-1150.

**[33]** McGuire MF. **Stainless Steels for Design Engineers.** ASM International, Materials Park, OH; 2008.

**[34]** **Standard Test Method for Guided Bend Test for Ductility of Welds.** 2006; **92**(Reapproved 2003):5-8.

**[35]** Das U, Das R, Toppo V, Muthukumaran S. **Experimental Study on Tensile and Bending Behavior of Friction Stir Welded Butt Joints of Dissimilar Aluminum Alloys.** *Materials Today: Proceedings* 2019; **18**:4717-4723.

**[36]** American Society of Mechanical Engineers. **Standard Test Methods for Bend Testing of Material for Ductility E290-14.** 2044:1-10.

**[37]** Ismail AH. **Experimental and Analytical Study of Bending Stresses and Deflections in Curved Beam Made of Laminated Composite Material.** *Al-Khwarizmi Engineering Journal* 2014; **10**(4):21-32.

**[38]** Obeidi MA, McCarthy E, Kailas L, Brabazon D. **Laser Surface Texturing of Stainless Steel 316L Cylindrical Pins for Interference Fit Applications.** *Journal of Materials Processing Technology* 2018; **252**:58-68.

**[39]** Dak G, Sirohi S, Pandey C. **Study on Microstructure and Mechanical Behavior Relationship for Laser-Welded Dissimilar Joint of P92 Martensitic and 304L Austenitic Steel.** *International Journal of Pressure Vessels and Piping* 2022; **196**:104629.

**[40]** Sirohi S, Gupta A, Pandey C, Vidyarthy RS, Guguloth K, Natu H. **Investigation of the Microstructure and Mechanical Properties of the Laser Welded Joint of P22 and P91 Steel.** *Optics and Laser Technology* 2022; **147**:107610.

**[41]** Sun FZ, Li Y, Tan WD, Pang M. **Effect of Laser Scanning Speed on the Thermal-Mechanical Coupling Field of Laser Remelting of Valve Seat.** *Optik* 2021; **225**:165776.